Korea-Australia Rheology Journal
Vol. 12, No. 3/4, December 2000 pp. 165-173

Three-dimensional numerical simulation of nonisothermal coextrusion process with generalized Newtonian fluids

Ki Byung Sunwoo, Seung Joon Park, Seong Jae Lee*, Kyung Hyun Ahn† and Seung Jong Lee†
School of Chemical Engineering, Seoul National University, Seoul 151-744, Korea
**Department of Polymer Engineering, The University of Suwon, Suwon 445-743, Korea*
(Received September 7, 2000; final revision received February 7, 2001)

Abstract

Three-dimensional numerical simulation of isothermal/nonisothermal coextrusion process of two immiscible polymers through a rectangular channel has been done using the finite element method. The encapsulation phenomenon with the less viscous layer encapsulating the more viscous layer was investigated with the generalized Newtonian fluids. The interface position around the symmetric plane obtained by numerical simulation nearly coincided with the one observed in experiments, but the degree of encapsulation was less than the one observed experimentally. Open boundary condition method was found to be applied to the simulation of nonisothermal coextrusion process, however, the results are not far from those using the fully developed boundary condition, because the temperature development along the downstream direction is very slow in the case of convection dominated flow. When the inlet velocity is increased, the interface profile does not change in isothermal flow, while it moves upward in nonisothermal situation. The degree of encapsulation decreases along the downstream direction in nonisothermal flow. When the inlet temperature increases compared to the wall temperature, the outlet interface moves downward and the degree of encapsulation increases. The difference of degree of encapsulation between the simulation and the experiments seems to arise from the viscoelastic effect of the materials. It was concluded that the nonisothermal effect alone does not explain the complex coextrusion process and the viscoelastic effect needs to be considered.

Keywords : coextrusion process, three-dimensional numerical simulation, finite element method, generalized Newtonian fluid, nonisothermal flow, open boundary condition

1. Introduction

Multicomponent extrusion process, known as coextrusion, has gained wide recognition as one of polymer processing to achieve unique product performance by combining the properties of different materials with lower costs. Typically, cylindrical dies are used in the production of conjugate and sheath-core fibers, and annular dies are used in the coextruded wire and cable or blown film industry. Multilayer polymer sheets or films are normally produced by the coextrusion of two or more polymers from flat dies. This is accomplished using either of two possible die configurations. In the first, the die is made up of manifolds for each polymer layer, and the layers are joined together just before they exit the die. In the second, one die is used for all layers and a coextrusion feedblock is used just prior to the entrance of the die. The purpose of the feedblock is to combine and distribute various layers such that they have a uniform thickness across the exit of the feedblock. Therefore, the design of both the feedblock and the die requires the understanding of three-dimensional flow behavior in the coextrusion process.

Experimental investigation of stratified flow in a side-by-side coextrusion has so far identified the viscosity difference between the polymer melts to be the controlling factor of the encapsulation phenomena, i.e. the less viscous melt wraps around the more viscous melt (Han, 1973; Lee and White, 1974; Southern and Ballman, 1975; Han and Kim, 1976). It occurs near the die walls and may result in undesirable product properties, which increases manufacturing cost due to the need to trim the film or sheet edges.

The modeling and simulation of coextrusion process require simultaneous consideration of mass, momentum, and energy conservation principles as well as constitutive relations. The complexity of die geometry and the nonlinear property of polymer melt result in a mathematical problem that must be solved numerically. Mavridis *et al.* (1987) implemented a double node technique for the stratified multiphase flow simulation to treat the discontinuity

†Corresponding author: ahnnet@snu.ac.kr and sjlee@plaza.snu.ac.kr

of pressure at the interface. Agassant and Fortin (1994), who tested the coextrusion process of Carreau fluids in two-dimensional formulation, pointed out that the interface location is strongly dependent on the flow rate and the flow rate ratio. However, they didnt make feasible description on the encapsulation phenomena. Karagiannis *et al.* (1990) and Gifford (1997) studied isothermal generalized Newtonian coextrusion process using a three-dimensional analysis.

This study focuses on the effects of processing variables and material property on the encapsulation phenomena in isothermal/nonisothermal coextrusion process of two immiscible fluids through a rectangular channel. In addition, the open boundary condition method to the nonisothermal simulation will be implemented.

2. Governing equations and numerical method

2.1. Governing equations

The bicomponent stratified flow of immiscible fluids involves the merging of two fluid streams, the flow inside the die, and the flow of the bicomponent system out of the die. In this study, the problem consists of the merging flow of two fluid streams and the interface shape development in the resulting bicomponent stratified flow inside the die.

Assuming incompressible, steady state, and creeping flow with no body forces, the three-dimensional forms of continuity, momentum and energy equations for the flow of two generalized Newtonian fluids (I and II) are

$$\nabla \cdot \boldsymbol{v}_k = 0, \qquad k = I,II \tag{1}$$

$$(\rho C_p)_k \boldsymbol{v}_k \cdot \nabla T_k = \kappa_k \nabla^2 T_k + \boldsymbol{\tau}_k : \nabla \boldsymbol{v}_k, \qquad k = I,II \tag{2}$$

$$\rho_k \boldsymbol{v}_k \cdot \nabla \boldsymbol{v}_k = -\nabla p_k + \nabla \cdot \boldsymbol{\tau}_k, \qquad k = I,II \tag{3}$$

where, $$\boldsymbol{\tau}_k = \eta_k(T, II_\Delta)\Delta_k = \eta_k(T, II_\Delta)(\nabla \boldsymbol{v}_k + \nabla \boldsymbol{v}_k^T), \tag{4}$$

$$II_\Delta = tr(\Delta^2), \tag{5}$$

$$\eta(II_\Delta) = \eta_o\left(1 + \left[\lambda\left(\frac{II_\Delta}{2}\right)^{\frac{1}{2}}\right]^2\right)^{\frac{n-1}{2}} \tag{6}$$

$$\eta_o(T) = K \exp\left(\beta\left(\frac{1}{T} - \frac{1}{T_0}\right)\right) \tag{7}$$

The boundary conditions at the interface are expressed as follows.

Kinematic conditions:

$$\boldsymbol{n} \cdot \boldsymbol{v}_I = \boldsymbol{n} \cdot \boldsymbol{v}_{II} = 0, \tag{8}$$

$$\boldsymbol{t}_1 \cdot \boldsymbol{v}_I = \boldsymbol{t}_1 \cdot \boldsymbol{v}_{II}, \tag{9}$$

$$\boldsymbol{t}_2 \cdot \boldsymbol{v}_I = \boldsymbol{t}_2 \cdot \boldsymbol{v}_{II} \tag{10}$$

Dynamic conditions:

$$\boldsymbol{t}_1 \cdot \boldsymbol{\sigma}_I = \boldsymbol{t}_1 \cdot \boldsymbol{\sigma}_{II}, \tag{11}$$

$$\boldsymbol{t}_2 \cdot \boldsymbol{\sigma}_I = \boldsymbol{t}_2 \cdot \boldsymbol{\sigma}_{II}, \tag{12}$$

$$\boldsymbol{n}_2 \cdot \boldsymbol{\sigma}_I - \boldsymbol{n}_2 \cdot \boldsymbol{\sigma}_{II} = 0 \tag{13}$$

The flow domain is discretized into 27-node hexahedron elements, and the Galerkin finite element procedure is applied as described in Lee and Lee (1990).

2.2. Discontinuity of pressure

The pressure discontinuity at the interface is handled by assigning two pressure variables per every single node along the interface, which is called as a double node technique (Mavridis *et al.*, 1987; Karagiannis *et al.*, 1990). In double node approach, two pressure variables are assigned at each relevant vertex of the three-dimensional elements along the interface. Pressure is continuous within each of the fluid phases but double-valued, and therefore, discontinuous across the fluid/fluid interface.

2.3. Interface update scheme and remeshing procedure

The problem is complicated because of the existence of the fluid/fluid interface whose position is not known a priori and an interface update scheme must be included in the iterative calculation. Pathline method is used to update the interface position (Marvridis *et al.*, 1987; Karagiannis *et al.*, 1990; Gifford, 1997). The interface is described by the path of particles traveling downstream from the end of the separation plate because particles at the interface remain in a tangential direction to the interface. Their paths are determined by the relationship

$$\frac{u}{dx} = \frac{v}{dy} = \frac{w}{dz} \tag{14}$$

and the interface is calculated separately from the calculation of velocity field based on the latest information of converged velocity as follows:

$$\Delta y = \int \frac{v}{w} dz \tag{15}$$

The pathline method is a simple method but gives slow convergence, and thus the procedure generally needs a large number of iterations to achieve a specified convergence.

After updating the interface position, remeshing procedure is required. Only the flow domain in thickness direction is reconstructed from the predetermined ratio. The inner nodes are located on a set of straight spines: their distance to the upper wall is based on a proportionality factor that is constant throughout the deformation of the mesh. The coordinates of the inner nodes are thus directly related to the displacement of the interface nodes.

2.4. Determination of contact line

The existence of three-phase static contact lines, where the interface between the two fluids meets the die wall, adds a further complication to the three-dimensional analysis. The location of the fluid/fluid/solid contact line is not known a priori and thus a scheme to determine the contact points must be included in the numerical problem (Karagiannis *et al.*, 1990; Torres *et al.*, 1993). In this work, the quadratic extrapolation method for the determination of the contact point is used for simplicity. In reality, the effect of extrapolation order is very small in case of the refined mesh around the wall contact line. This extrapolation technique is the simplest method to obtain the location of the contact line, but does not consider the exact wall effect.

2.5. Open boundary condition method

In the numerical simulation of nonisothermal flow inside a die, it is almost impossible to impose the outflow velocity and temperature profiles correctly. The ambiguous imposition of the outflow boundary condition can be avoided by using the open boundary condition method (Park and Lee, 1999; Sunwoo *et al.*, 2000). Open boundary condition method allows the solution to pass through the outflow boundary without undergoing significant distortion and influencing the interior solution.

3. Numerical results and discussion

3.1. Determination of Contact Line

Firstly, the outlet interface profiles near the wall with different extrapolation orders are compared in Fig. 1, where the shear viscosity ratio ($K_{upper\ layer}/K_{lower\ layer}$) is 5.0, the flow rate ratio ($Q_{upper\ layer}/Q_{lower\ layer}$) is 1.0, and the average inlet velocity is 5.0 cm/s. The interface shapes are nearly the same when the extrapolation orders are greater than two. Thus, quadratic extrapolation method is used throughout this work for simplicity.

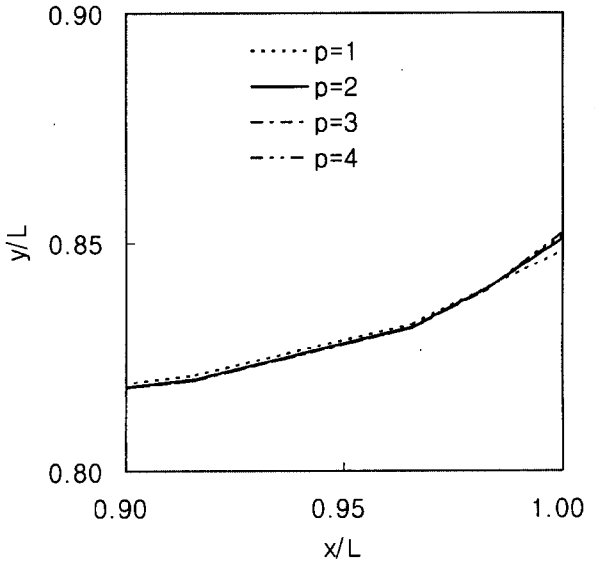

Fig. 1. Effect of extrapolation order near the contact line (Mesh2, K_{IV}/K_{III}=5.0, Q_{IV}/Q_{III}=1.0, <w>=5.0 cm/s).

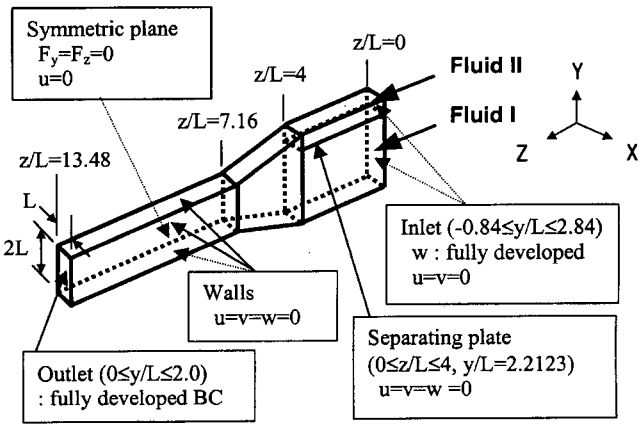

Fig. 2. Die geometry and imposed boundary conditions for isothermal simulation.

3.2. Isothermal coextrusion

The die geometry and boundary conditions used for isothermal generalized Newtonian coextrusion process are shown in Fig. 2. The two fluids flowing in the rectangular die are initially separated by the flat separating plate ($0 \le z/L \le 4$, y/L=2.2123) followed by converging section ($4 < z/L < 7.16$). The upper fluid (Fluid II) is less viscous ($\eta_{o,I}/\eta_{o,II} \approx 2.64$) and has lower flow rate (Q_I/Q_{II}=13.2) than the lower fluid (Fluid I). The average inlet velocities of the lower and upper fluid are 9.137 and 3.365, respectively. The fully developed velocity profile and condition are imposed on the inlet and outlet planes, respectively. The finite element mesh used in this study is shown in Fig. 3 as

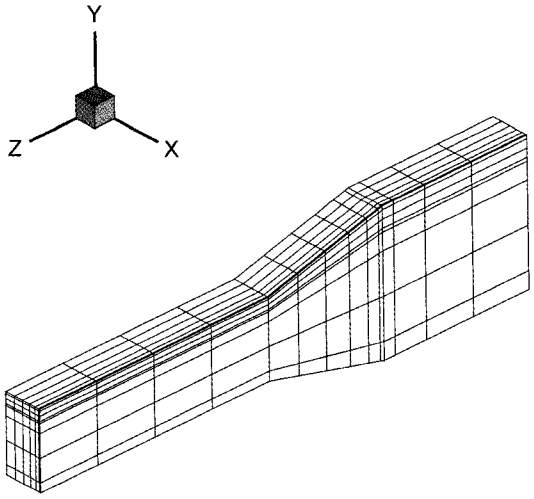

Fig. 3. Finite element mesh used in isothermal simulation (Mesh1).

Table 1. Material parameters for polystyrenes used in the simulation of generalized Newtonian coextrusion process. The data are taken from Karagiannis *et al.* (1990) and typical values of polystyrene

	Fluid I (Dow Styron™ 472)	Fluid II (Dow Styron™ 678E)
Zero shear viscosity (K) at 220°C	1,461 Pa·s	553 Pa·s
Relaxation time (λ)	0.040 sec	0.015 sec
Power index (n)	0.36	0.31
Constant β in Arrhenius type equation	12,236 K	
Density (ρ)	997 kg/m^3	
Thermal conductivity (κ)	0.167 W/m·K	
Specific heat capacity (Cp)	2,040 J/kg·K	

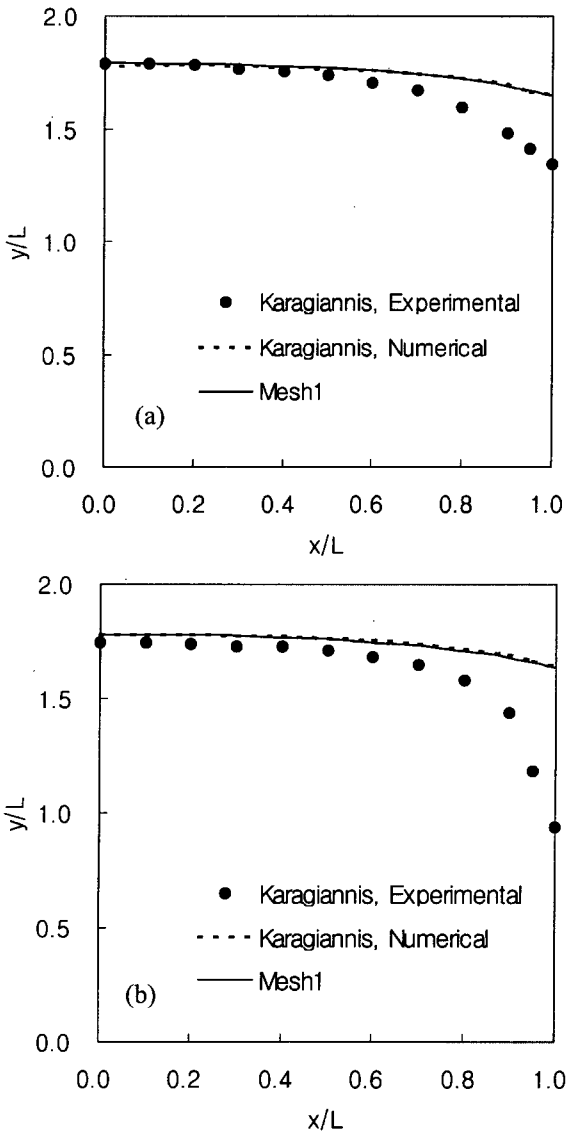

Fig. 4. Interface profile (Mesh1, $\eta_{o,I}/\eta_{o,II} \approx 2.64$, Q_I/Q_{II}=13.2); (a) z/L=8 (b) z/L=12.

Mesh1. The number of elements and nodes are 672 and 6786, respectively. The Carreau model was employed to fit the shear thinning viscosity data of two polystyrenes used by Karagiannis *et al.* (1990). The fitted parameters are presented in Table 1.

In Fig. 4, the interface profiles are compared. It can be seen that the less viscous Fluid II tends to encapsulate the more viscous Fluid I. The result from this study coincides closely with the numerical result of Karagiannis *et al.* (1990), but shows less encapsulation compared to the experimental result of Karagiannis *et al.* (1990). The experimental result shows the increase of encapsulation along the downstream direction, but the results obtained by numerical simulation hardly show such an increase of encapsulation. That increase may be explained and obtained by numerical simulation using the viscoelastic constitutive relation, which has non-zero second normal stress difference as shown by Takase *et al.* (1998) and Sunwoo *et al.* (2000). Nevertheless, the interface positions around the symmetric plane nearly coincide.

3.3. Nonisothermal coextrusion

The geometry and boundary conditions used for the nonisothermal simulation of generalized Newtonian fluids are shown in Fig. 5. The two fluids flowing in the rectangular die are initially separated by the flat separating plate ($0 \leq z/L \leq 4$, y/L=1.0). The upper fluid (Fluid IV) is more viscous (K_{IV}/K_{III}=5.0) than the lower fluid (Fluid III) and has the same flow rate (Q_{IV}/Q_{III}=1.0) with the lower fluid. After imposing the fully developed velocity profile and constant temperature on the inlet plane, the results under two types of outlet boundary conditions will be compared: the fully developed boundary condition (FBC) and the open boundary condition (OBC). The finite element mesh used in this case is shown in Fig. 6 as Mesh2, where the number of elements and nodes are the same with those of Mesh1. The Arrhenius type temperature dependency of zero shear viscosity was used and the parameters used in this study are presented in Table 2.

As a simple criterion for the encapsulation phenomena, the degree of encapsulation is defined as

Table 2. Material parameters for LDPE used in the simulation of generalized Newtonian coextrusion process. The data are taken from Luo and Tanner (1987) and typical values of LDPE

	Fluid III	Fluid IV
Zero shear viscosity [a] (K) at 150°C	11,000 Pa·s	55,000 Pa·s
Relaxation time [b] (λ)	0.015 sec	
Power index [b] (n)	0.31~1.00	
Constant β in Arrhenius type equation	8,000 K	
Density (ρ)	782 kg/m^3	
Thermal conductivity (κ)	0.260 W/m·K	
Specific heat capacity (Cp)	2,302 J/kg·K	

[a] The zero shear viscosity of Fluid III was set to one fifth of Fluid IV to give the smaller viscosity different from Fluid IV intentionally.
[b] We set the relaxation time in Carreau model arbitrarily and varied the power index from 1.0 to 0.31.

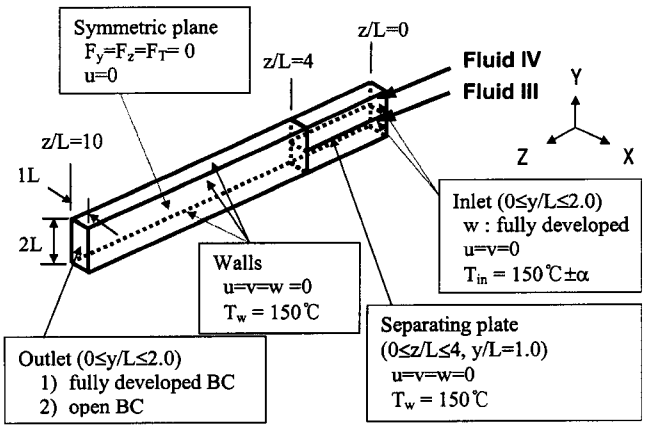

Fig. 5. Die geometry and imposed boundary conditions for nonisothermal simulation.

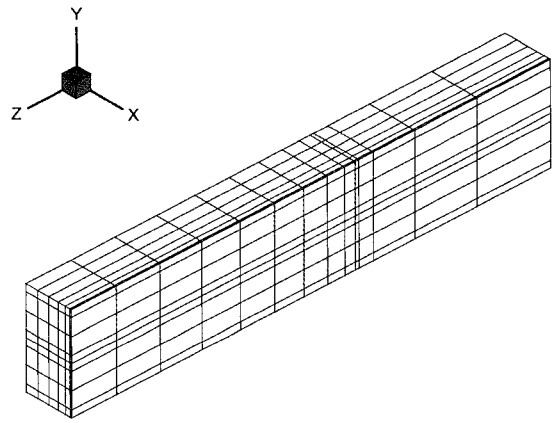

Fig. 6. Finite element mesh used in nonisothermal simulation (Mesh2).

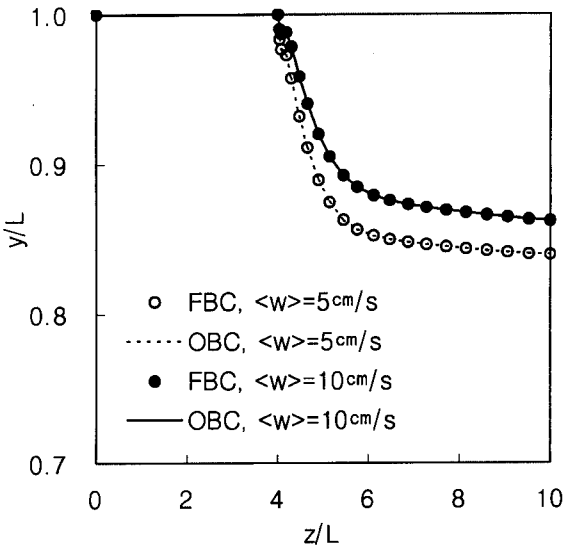

Fig. 7. Contact line positions along the downstream direction with different outlet boundary conditions (Mesh2, K_{IV}/K_{III}=5.0, Q_{IV}/Q_{III}=1.0, n=0.31, T_{in}=150°C).

$$\text{Degree of Encapsulation (DE)} = \frac{y_w - y_c}{L} \times 100\,(\%) \quad (16)$$

where y_w is the height of interface at side wall and y_c is the one at symmetric plane.

3.3.1. Effect of outlet boundary condition

Fig. 7 shows the contact line positions along the downstream direction under different outlet boundary conditions, where the results with the same inlet velocity nearly coincide. The slow development of temperature along the downstream direction in convection-dominated generalized Newtonian fluid flow (<w>=5 cm/sec (T_{in}=150°C, Pe=3,462) and <w>=10 cm/sec (T_{in}=150°C, Pe=6,924)) resulted in nearly the same contact line positions regardless of the fully developed boundary condition (FBC) or the open boundary condition (OBC). But, this can be generalized neither to the conduction-dominated flow nor to the viscoelastic fluid flow (Park and Lee, 1999; Sunwoo *et al.*, 2000).

3.3.2. Newtonian fluid

Figs 8 and 9 show the outlet interface profile and the degree of encapsulation along the downstream direction, respectively, with different average inlet velocities. The outlet interface profile does not change in isothermal flow even though the average inlet velocity increases. In nonisothermal flow, however, the outlet interface moves upward as the average inlet velocity increases. The viscous heating is larger in more viscous upper layer (Fluid IV), which causes large temperature rise as shown in Fig. 10 and the decrease of viscosity of Fluid IV. Therefore, the viscosity ratio ($\eta_{o,IV}/\eta_{o,III}$) decreases and the outlet interface moves upward. Along the downstream direction, the temperature near the side wall in the upper layer also increases as

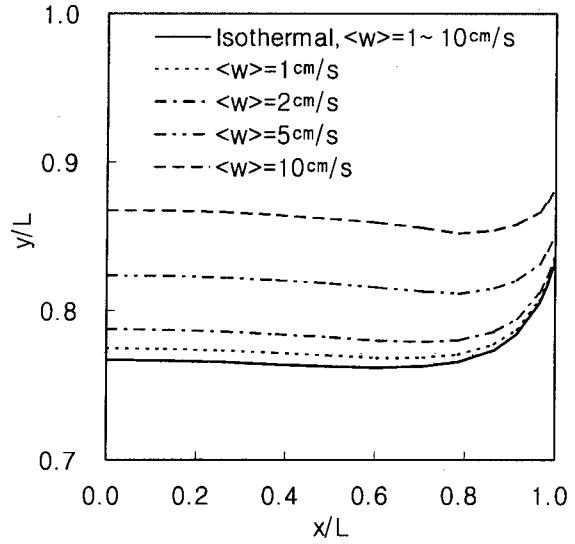

Fig. 8. Outlet interface profiles with different average inlet velocities (Mesh2, K_{IV}/K_{III}=5.0, Q_{IV}/Q_{III}=1.0, n=1.0, T_{in}=150°C).

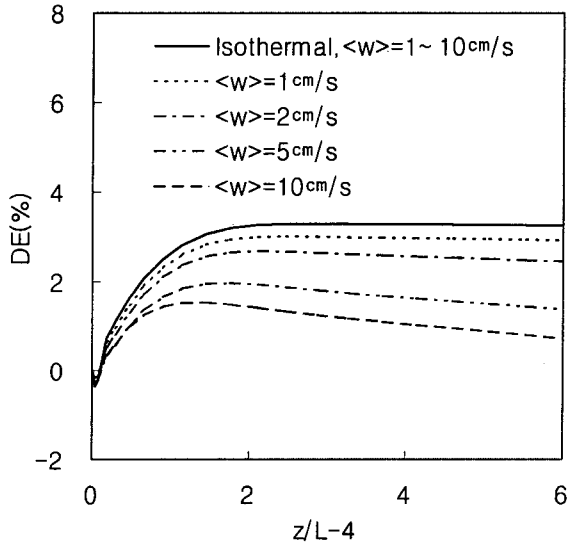

Fig. 9. Degree of encapsulations along the downstream direction with different average inlet velocities (Mesh2, K_{IV}/K_{III}=5.0, Q_{IV}/Q_{III}=1.0, n=1.0, T_{in}=150°C).

shown in Fig. 10 and this results in the decrease of viscosity ratio near the side wall. After all, the degree of encapsulation of Fluid III around Fluid IV decreases along the downstream direction as shown in Fig. 9.

In nonisothermal flow, the upward movement of the outlet interface and the decrease of the degree of encapsulation along the downstream direction can induce distorted outlet interface profile, and this tendency increases as the average inlet velocity increases as shown in Fig. 8.

3.3.3. Generalized newtonian fluid

Fig. 11 shows the outlet interface profile at various power indices (See Table 2). In isothermal flow, the average shear

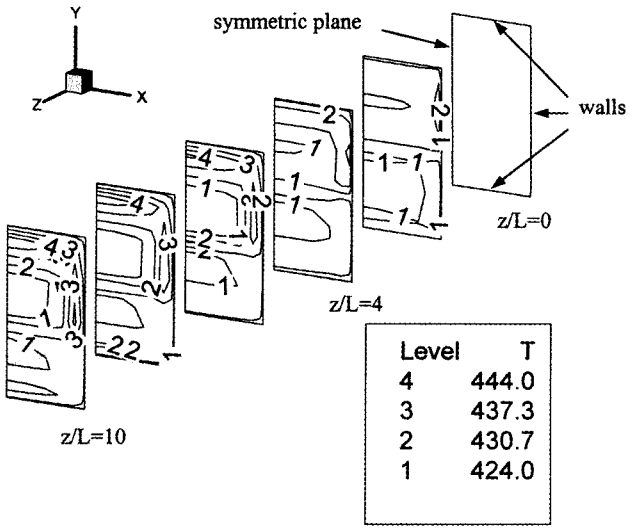

Fig. 10. Temperature contours at different downstream positions (Mesh2, K_{IV}/K_{III}=5.0, Q_{IV}/Q_{III}=1.0, <w>=5.0 cm/s, n=1.0, T_{in}=150°C).

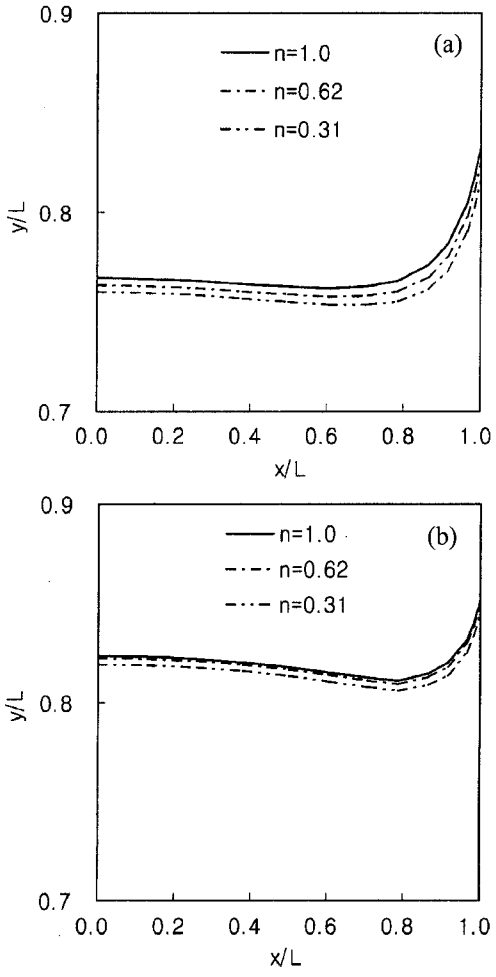

Fig. 11. Outlet interface profiles with different power indices (Mesh2, K_{IV}/K_{III}=5.0, Q_{IV}/Q_{III}=1.0, <w>=5.0 cm/s, T_{in}=150°C); (a) isothermal (b) nonisothermal.

rate of Fluid III is higher than that of Fluid IV, and the shear thinning effect is larger at high shear rate region than at low shear rate region when shear viscosity has shear rate dependency of Carreau model. Thus, the lowering of shear viscosity of Fluid III is larger than that of Fluid IV, and this results in the increase of the viscosity ratio (η_{IV}/η_{III}). The viscosity ratio increased more as the power index decreases. Therefore, the outlet interface moves downward due to the increase of the viscosity ratio as the shear thinning effect increases.

In nonisothermal flow, we should consider the effect of viscous heating together. The viscous heating of Fluid IV (more viscous layer) is larger than that of Fluid III (less viscous layer), and the lowering of shear viscosity of Fluid IV due to viscous heating is larger than that of Fluid III. Thus, the viscosity ratio decreases compared to the one in isothermal case. Therefore, the effect of viscous heating works in opposite direction to the shear thinning effect and the outlet interface position in nonisothermal case moves upward compared to the one in isothermal case as shown in Fig. 11. The lowering effect of the viscosity ratio in nonisothermal case increases as the shear thinning effect of viscosity increases because of the increased average shear rate of Fluid IV. Thus, the downward movement of outlet interface the decrease of the power index in nonisothermal simulation is smaller than that in isothermal simulation.

3.3.4. Effect of inlet temperature

As the inlet temperature increases compared to the wall temperature, the outlet velocity increases near the center region (x/L=0) and decreases near the side wall (x/L=1.0) as shown in Fig. 12. The increased temperature near the center region induces the lowering of shear viscosity, and therefore the velocity increases. Near the side wall, the temperature decreases than the one near the center region by the cooling effect of lower wall temperature and thus the velocity decreases due to the increased shear viscosity. When the inlet temperature is lower than the wall temperature, the inverse tendency is observed.

As already mentioned, the average shear rate of Fluid III is higher than that of Fluid IV, and thus the lowering of shear viscosity of Fluid III is larger than that of Fluid IV. This tendency increases as the velocity increases with increased inlet temperature. Thus, the viscosity ratio (η_{IV}/η_{III}) near the center region increases as the inlet temperature increases. For example, the viscosity ratio at the outlet center point increased from 12.1 to 13.9 as the inlet temperature increased 60°C higher than the wall temperature. Therefore, the outlet interface moves downward with the increase of inlet temperature as shown in Fig. 13. The effect of viscous heating near the side wall decreases as the inlet temperature increases and this results in the increased encapsulation. When the inlet temperature decreases compared to the wall temperature, the inverse tendency is observed also in the outlet interface profile.

3.4. Nonisothermal coextrusion in mesh1

As mentioned earlier, the numerical results with isothermal analysis show less encapsulation than that by experimental observation. Here, we studied the effect of viscous heating in Mesh1 with nonisothermal analysis, where the thermal data of typical polystyrene were used as given in Table1, and the same process conditions were used as in the experiment of Karagiannis *et al.* (1990). We imposed constant temperature (220°C) at the inlet plane and walls, and imposed open boundary condition (OBC) at the outlet plane.

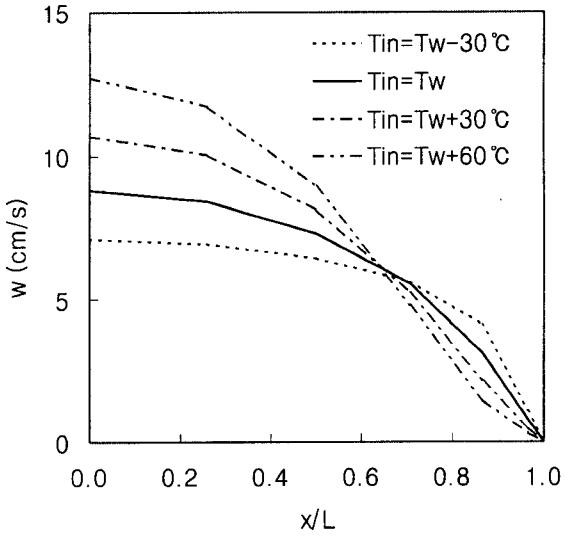

Fig. 12. Velocity profiles at the outlet interface with different inlet temperatures (Mesh2, K_{IV}/K_{III}=5.0, Q_{IV}/Q_{III}=1.0, <w> =5.0 cm/s, n=0.31).

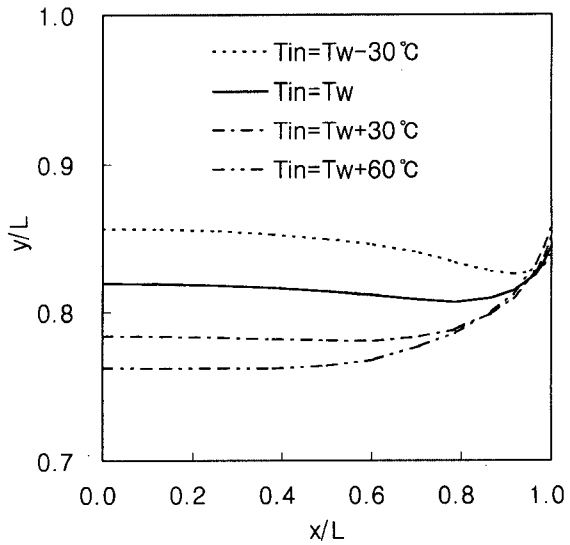

Fig. 13. Outlet interface profiles with different inlet temperatures (Mesh2, K_{IV}/K_{III}=5.0, Q_{IV}/Q_{III}=1.0, <w>=5.0 cm/s, n=0.31).

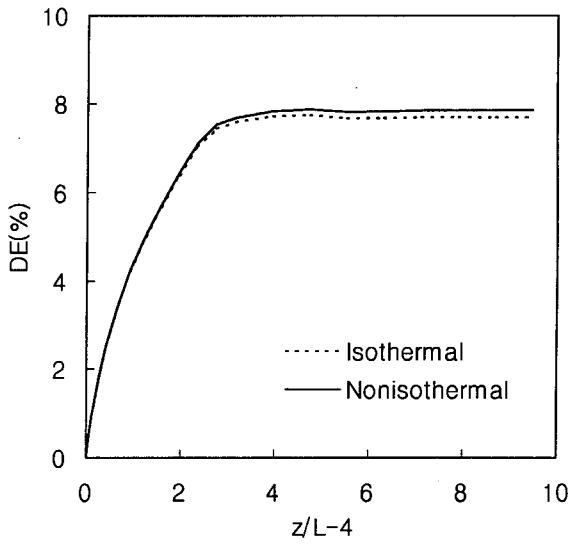

Fig. 14. Degree of encapsulations along the downstream direction with Mesh1 ($K_I/K_{II} \approx 2.64$, Q_I/Q_{II}=13.2).

The degree of encapsulation along the downstream direction with viscous heating is shown in Fig. 14. The viscous heating in this case is complex due to the factors such as contraction zone ($4<z/L<7.16$), large flow rate ratio ($Q_I/Q_{II} = 13.2 \gg 1$), different average inlet velocity ($<w_I>=$ 9.137 cm/sec, $<w_{II}>=$ 3.365 cm/sec) and the height of separating plate (y/L=2.2123 >1.0), etc. The resulting effect of viscous heating is small increase of degree of encapsulation, but that was too small to follow the experimental data. The difference of degree of encapsulation between the numerical results and the one observed experimentally cannot be explained by the viscous heating effect alone. That should be interpreted by the effect of viscoelastic properties such as the elasticity and non-zero second normal stress difference (Takase *et al.*, 1998; Sunwoo *et al.*, 2000).

4. Conclusions

A three-dimensional, isothermal/nonisothermal finite element code was developed to study the encapsulation phenomena in bicomponent stratified coextrusion process of generalized Newtonian fluids. The interface position around the symmetric plane obtained by numerical simulation nearly coincided with the one observed in experiment by Karagiannis *et al.* (1990), but the degree of encapsulation was less than the one observed experimentally.

We found that the open boundary condition method can be applied to the simulation of nonisothermal coextrusion process. The result using the open boundary condition at the outlet showed little difference from that using the fully developed boundary condition because the temperature development along the downstream direction is very slow in the case of convection dominated flow (high Peclet number).

The interface profile does not change despite the increasing average inlet velocity in isothermal flow. In nonisothermal flow, however, the interface profile has moved upward due to the decrease of viscosity ratio, which resulted from larger viscous heating in the higher viscous upper layer. The degree of encapsulation also decreased along the downstream direction because of the decreased viscosity ratio caused by the continuous viscous heating near the side wall of the upper layer.

The outlet interface moved downward as shear thinning effect increases, and this tendency decreased when the viscous heating was considered. We can conclude that the effect of viscous heating works in opposite direction to the shear thinning effect of viscosity.

As the inlet temperature increased compared to the wall temperature, the increased velocity near the center region due to the high inlet temperature and the decreased velocity near the side wall due to the cooling effect by the lower wall temperature were observed. And, the outlet interface moved downward and the increased encapsulation was observed.

When the viscous heating is included in the simulation with Mesh1, the degree of encapsulation increased very small amount. So, the resulting degree of encapsulation was still not enough to follow the experimental data. The difference of degree of encapsulation with the one observed experimentally cannot be explained by the viscous heating effect alone but should be interpreted by the effect of viscoelastic properties.

Acknowledgement

The authors wish to acknowledge the financial support of Honam Petrochemical Corporation in Korea. This work was also partially supported by the Brain Korea 21 project.

List of symbols

Alphabetic symbols

$\boldsymbol{v}$	: velocity vector
T	: temperature
T_{in}	: inlet temperature
T_w	: wall temperature
C_p	: specific heat capacity
II_Δ	: second invariant of deformation tensor
p	: pressure
K	: zero shear viscosity at reference temperature in Carreau model
n	: power index in Carreau model
$\boldsymbol{n}$	: unit normal vector at the interface
$\boldsymbol{t}$	: unit tangential vector at the interface

L : characteristic length
x, y, z : x-, y-, and z-coordinate direction
u, v, w : x, y-, and z-velocity component
$\langle w \rangle$: average velocity at the inlet
y_w : height of interface at side wall
y_c : height of interface at symmetric plane
Q : volumetric flow rate
Pe : Peclet number

Greek symbols

β : constant related to the activation energy of the material
ρ : density
κ : thermal conductivity
η : viscosity
λ : relaxation time in Carreau model
τ : extra stress
σ : total stress
Δ : rate of deformation tensor
∇ : gradient operator

References

Agassant, J. F. and A. Fortin, 1994, Prediction of stationary interfaces in coextrusion flows, *Polym. Eng. Sci.* **34**, 1101.

Gifford, W. A., 1997, A three-dimensional analysis of coextrusion, *Polym. Eng. Sci.* **37**, 315.

Han, C. D. 1973, A study of bicomponent coextrusion of molten polymers, *J. Appl. Polym. Sci.* **17**, 1289.

Han, C. D. and Y. W. Kim, 1976, Further observations of the interface shape of conjugate fibers, *J. Appl. Polym. Sci.* **20**, 2609.

Karagiannis, A., A. N. Hrymak and J. Vlachopoulos, 1990, Three-dimensional studies on bicomponent extrusion, *Rheol. Acta* **29**, 71.

Lee, B. L. and J. L. White, 1974, An experimental study of rheological properties of polymer melts in laminar shear flow and interface deformation and its mechanism in two-phase stratified flow, *Trans. Soc. Rheol.* **18**, 467.

Lee, S. J. and S. J. Lee, 1990, Numerical prediction of three-dimensional extrudate swell, *Kor. J. Rheol.* **2**, 35.

Mavridis, H., A. N. Hrymak and J. Vlachopoulos, 1987, Finite-element simulation of stratified multiphase flows, *AIChE J.* **33**, 410.

Minagawa, N. and J. L. White, 1975, Co-extrusion of unfilled and TiO2-filled polyethylene: Influence of viscosity and die cross-section on interface shape, *Polym. Eng. Sci.* **15**, 825.

Park, S. J. and S. J. Lee, 1999, On the use of the open boundary condition method in the numerical simulation of nonisothermal viscoelastic flow, *J. Non-Newtonian Fluid Mech.* **87**, 197.

Southern, J. H. and R. L. Ballman, 1975, Additional observations on stratified bicomponent flow of polymer melts in a tube, *J. Polym. Sci.* **13**, 863.

Sunwoo, K. B., S. J. Park, S. J. Lee, K. H. Ahn and S. J. Lee, 2000, Numerical simulation of three-dimensional viscoelastic flow using the open boundary condition method in coextrusion process, *J. Non-Newtonian Fluid Mech.* (in preparation).

Takase, M., S. Kihara and K. Funatsu, 1998, Three-dimensional viscoelastic numerical analysis of the encapsulation phenomena in coextrusion, *Rheol. Acta* **37**, 624.

Torres, A., A. N. Hrymak, J. Vlachopoulos, J. Dooley and B. T. Hilton, 1993, Boundary conditions for contact lines in coextrusion flows, *Rheol. Acta* **32**, 513.